Computer Methods and Programs in Biomedicine 197 (2020) 105726

Contents lists available at ScienceDirect

Computer Methods and Programs in Biomedicine

journal homepage: www.elsevier.com/locate/cmpb

Dyslexia detection using 3D convolutional neural networks and functional magnetic resonance imaging

Sofia Zahia[a,*], Begonya Garcia-Zapirain[a], Ibone Saralegui[b], Begoña Fernandez-Ruanova[c]

[a] eVida research laboratory, University of Deusto, Bilbao 48007, Spain
[b] Department of Neuroradiology, Osatek, Biocruces-Bizkaia; Galdakao-Usansolo Hospital / Osakidetza, Galdakao 48960, Spain
[c] Research and innovation Department, Osatek, Biocruces-Bizkaia; Osakidetza, Bilbao 48011, Spain

ARTICLE INFO

Article history:
Received 3 August 2019
Accepted 22 August 2020

Keywords:
Deep learning
Dyslexia
Functional magnetic resonance Imaging
3D Convolutional Neural Networks
Computer-aided diagnosis (CAD)

ABSTRACT

Background and Objectives: Dyslexia is a disorder of neurological origin which affects the learning of those who suffer from it, mainly children, and causes difficulty in reading and writing. When undiagnosed, dyslexia leads to intimidation and frustration of the affected children and also of their family circles. In case no early intervention is given, children may reach high school with serious achievement gaps. Hence, early detection and intervention services for dyslexic students are highly important and recommended in order to support children in developing a positive self-esteem and reaching their maximum academic capacities. This paper presents a new approach for automatic recognition of children with dyslexia using functional magnetic resonance Imaging. **Methods**: Our proposed system is composed of a sequence of preprocessing steps to retrieve the brain activation areas during three different reading tasks. Conversion to Nifti volumes, adjustment of head motion, normalization and smoothing transformations were performed on the fMRI scans in order to bring all the subject brains into one single model which will enable voxels comparison between each subject. Subsequently, using Statistical Parametric Maps (SPMs), a total of 165 3D volumes containing brain activation of 55 children were created. The classification of these volumes was handled using three parallel 3D Convolutional Neural Network (3D CNN), each corresponding to a brain activation during one reading task, and concatenated in the last two dense layers, forming a single architecture devoted to performing optimized detection of dyslexic brain activation. Additionally, we used 4-fold cross validation method in order to assess the generalizability of our model and control overfitting. **Results**: Our approach has achieved an overall average classification accuracy of 72.73%, sensitivity of 75%, specificity of 71.43%, precision of 60% and an F1-score of 67% in dyslexia detection. **Conclusions**: The proposed system has demonstrated that the recognition of dyslexic children is feasible using deep learning and functional magnetic resonance Imaging when performing phonological and orthographic reading tasks.

1. Introduction

Dyslexia is a brain based condition which impacts reading, writing and spelling. It is the most prevalent learning disability [1]. Dyslexia is defined by the international classification ICD-10 as "A cognitive disorder characterized by an impaired ability to comprehend written and printed words or phrases despite intact vision" (2019 ICD-10-CM Diagnosis Code F81.0). Unfortunately, dyslexia is a genetic life long issue which tends to run through family members, and may lead to the social exclusion of the affected person if it is not addressed properly. It is necessary to assert that dyslexia does not have to do with intelligence. Children with dyslexia are just as smart as other children with functional reading and writing abilities.

Related researches have shown that dyslexia's central difficulty indicates a deficit in language system (Phonological theory [3–6]). However, other theoretical sources remain cogent, such as the Cerebellar theory [8], the Magnocellular visual deficit theory of dyslexia [14–16], the Auditory temporal processing deficit theory [7], and the Visual attention span deficit theory [9–12].

Measuring phonological skills does not efficiently distinguish dyslexics, who have difficulties learning to read and translating letters into phonemes, from all the other children not able to read

* Corresponding author.
E-mail address: sofia.zahia95@deusto.es (S. Zahia).

https://doi.org/10.1016/j.cmpb.2020.105726

for other reasons such as a poor teaching, general family stress and lack of their support, etc... Besides, abnormal eye tracking has also been mistakenly suspected as being a cause in reading problems. In fact, people with little to no ability to move their eyes still can demonstrate normal reading abilities [2]. Hence, studies have been conducted to have a closer look at the functional differences in brain activation during reading tasks [13,17]. In the study done by Saralegui et al. [17], a comprehensive fMRI analysis including three different cognitive tasks was conducted: a task of lexical decision where children had to answer whether the word was real or did not exist, and orthographic matching task where they had to answer if the two displayed words were identical or not, and semantic categorization task where they were asked to detect whether all the displayed words belonged to the same semantic category. In that way, the pathways of language were explored in order to reproduce the neural network involved in reading. The results showed that, while reading, the pattern of activation of control children and children with monocular vision were similar, and both of them seemed different from those of dyslexic children. In fact, dyslexic children have less activation in the left Wernicke's area, both Broca's areas and the posterior part of the visual word form area, which are all located in the left hemisphere and are associated to the phonological route. And to counteract for this deficit, dyslexics tend to have more activation in the anterior part of the VWFA as well as the posterior part of both MTG, which are associated with the orthographic route, compared to non dyslexic readers. Hence, using this disclosure, we decided to conduct this study and detect dyslexic children using a classification of brain activation with functional Magnetic Resonance Imaging (fMRI).

Meanwhile, during the last decades, artificial intelligence has gained a lot of popularity thanks to its successful real-world application results. Deep learning has enabled an optimal representation of data for the problems at hand. The models of Deep learning are merely built of cascaded layers which transform the input data to desired outputs while learning their higher level features [45]. Convolutional Neural Networks (CNNs), also known as ConvNets, are feed-forward neural networks composed of a sequence of convolution and pooling layers, optionally followed by fully connected layers. They are the most efficient type of models for image analysis and have been proven to be very adequate for object detection [43,44], pattern recognition and image segmentation [46,47], and more precisely in medical imaging. For instance: Brain image analysis (Disorder classification [18,19], tissue/anatomy/lesion/tumor segmentation [20–22], survival/disease activity/development prediction [23], image construction/enhancement [24,25]), Chest (x-ray and CT images) [27–29], abdominal [30], cardiac [31,32], dermatological [33–35], etc... These architectures can also be applied on 3D images and thus are called 3D CNNs. The latest research has proven that these architectures efficiently enable the segmentation or classification of diseases from medical volumes and stacked scans such as multi-channel MRI patient data as presented by Kamnitsas et al. [48]. In this paper, the authors present DeepMedic, a 3D CNN architecture for automatic brain lesion segmentation that outperformed the state-of-the-art techniques on challenging data. Dolz et al. [49] demonstrated also the usability of 3D CNN for the subcortical brain structure segmentation using MRI scans. As for classification, the work by Lian, Zou et al. [42] demonstrated the efficiency of 3D CNN model to detect people with Attention deficit hyperactivity disorder (ADHD) using MRI scans. Their approach achieved the state-of-the-art accuracy of 69.15% and outperformed the methods in the literature. Also, schizophrenia detection was conducted by Qureshi et al. [52] and Oh, Kanghan, et al. [53]. Both studies asserted that 3D CNN models were the best performing models, far more than what classical machine learning methods achieved, even on limited datasets. Furthermore, 3D CNNs have been applied on other medical volumes such as chest CT scans for lung nodule detection, as presented by Gu, Yu et al. [50], or pulmonary nodules classification presented by Jiang, H. et al. [51]. Based on these promising results of this architecture, we decided to use the 3D convolutional neural networks to solve the classification problem in hand. Hence, our approach consists in developing a deep learning architecture based on parallel 3D CNN applied on the three volumes containing the brain activation areas during each one of the three reading paradigms.

The rest of this paper is constructed as follows: Section II.A will discuss the dataset used for this study including participants and data acquisition protocol. Section II.B will discuss the proposed framework which is composed of a preprocessing step followed by the designed 3D CNN architecture. In Section III, we will present the validation metrics and discuss the experiment results of the proposed method. Finally, Section IV will conclude this paper.

2. Materials and methods

This section presents the dataset used to conduct this research, and our proposed approach to detect children with dyslexia from the analysis of their brain areas of activation.

2.1. Dataset

2.1.1. Participants

A total of number of 66 children aged between 9 and 12 years were recruited from the University Hospital of Cruces paediatric ophthalmology and neurology departments, as well as schools also in Bilbao (Spain) in the case of control children. Additionally, the recruited participants were all Spanish and right-handed.

Children were distributed in three different groups: Control group (TDR), Dyslexia group (DXR) and Monocular vision group (MVR), conforming to the exclusion and inclusion criteria listed below:

Inclusion criteria: Dyslexic children were admitted in the study only when they had a diagnosis of dyslexia and did not receive treatment or psycho-pedagogical help for literacy. The Wechsler Intelligence Scale - Fourth edition (WISC-IV) score also needed to show that their Intelligence Quotient (IQ) fell within the normal range, (>75). The participants within the monocular vision group did not show any reading disabilities, and those of control group did not show any literacy weakness due to ocular pathology.

Exclusion criteria: Participants were not allowed to join the study if they had previously one of the following diseases: a neurological disease or serious head trauma, psychiatric illness, impaired sensory-motor coordination, chronic drug treatment, inadequate schooling, social deprivation or intolerance to MRI scanning (claustrophobia, lack of cooperation, etc.). Dyslexic children were screened to check the presence of any vision or motility abnormality, and only subjects with refractive error were admitted after their diagnosed abnormality was corrected with normal visual acuity.

After checking the concordance of the participants with the inclusion and exclusion criteria stated above, 55 children were finally accepted to take part in the study. They were divided into the three groups as follows: Dyslexia group, 19 (8 female); Monocular Vision group, 17 (8 female); Control group, 19 (8 female), as shown in Table 1.

This research was constantly conducted in agreement with the Code of Ethics of the World Medical Association (Declaration of Helsinki) and requirements specified by the Galdakao Hospital Ethics Committee of Clinical Research. Authentically, the children joined the study after their parents and guardians received and signed an informed written consent which explained the aims and protocols of the study.

Table 1
Participants' characteristics [17].

	TDR	DXR	MVR	p*
Sample size	19	19	17	
Age (years)**	10 ± 0.9 (9-12)	10.5 ± 1.1 (9-12)	10.4 ± 0.9 (9-12)	0.220
Gender (Female/Male)	8/11	8/11	7/10	0.998
Attention deficit hyperactivity disorder	2	2	1	0.858
Corrected visual acuity	1	1	1	
IQ**				
Full scale	108.3 ± 12.0 (92-131)	94.6 ± 14.3 (76-126)	103.1 ± 7.7 (90-113)	0.004
Verbal comprehension index	110.6 ± 14.0 (91–134)	91.0 ± 15.5 (65–123)	101 ± 10.8 (83–126)	<0.001
Perceptual reasoning index	107.4 ± 10.3 (87–123)	101.0 ± 19.8 (65–132)	103.5 ± 13.1 (76–124)	0.455
Processing speed index	97.2 ± 9.5 (85–119)	96.5 ± 7.9 (82–112)	101.9 ± 10.9 (79–121)	0.179
Working memory index	104.9 ± 9.3 (88–127)	96.4 ± 16.1 (68–122)	107.1 ± 9.8 (91–125)	0.094
BASC (range)	40–60	40–60	40–60	
Reading score (PROLEC-R)**				
Word reading accuracy (n/40)	39.6 ± 0.7 (38–40)	36.0 ± 3.3 (28–40)	39.8 ± 0.7 (38–40)	<0.001
Pseudoword reading accuracy (n/40)	37.2 ± 1.7 (34–40)	30.3 ± 5.4 (19–38)	36.5 ± 1.8 (33–39)	<0.001
Word reading speed (s)	41.1 ± 8.3 (22–58)	82.5 ± 49.0 (32–186)	31.9 ± 12.3 (17–58)	<0.001
Pseudoword reading speed (s)	68.3 ± 15.4 (47–102)	99.2 ± 51.3 (57–229)	58.4 ± 19.0 (23–104)	0.006
Word reading skill (accuracy/speed) × 100	101.6 ± 25.7 (67–182)	60.6 ± 30.9 (15–119)	144.3 ± 45.9 (65–235)	<0.001
Pseudoword reading skill (accuracy/speed)x100	57.5 ± 12.1 (39-81)	38.3 ± 17.5 (9-65)	70.6 ± 25.1 (33-143)	<0.00

*Kruskal-Wallis H or Pearson's chi-square test. **The values are mean ± SD (max-min) TDR: Control group,DXR: Dyslexia group, MVR: Monocular Vision group

2.1.2. Data acquisition

In order to acquire quality data, the children were shown the three different reading tasks, and were introduced to the entire procedure of the cognitive testing. The three paradigms conducted during this study were:

- **Lexical decision task**: The children were asked during this task to read two-syllable real words or pseudowords (which do not have actual meaning). Ten words were randomly presented, each one appearing every 3 s. The child had to read the word and decide whether it is a real word by pressing a button of the answering box that he/she has in the right hand, or a pseudoword by pressing the one in the left hand.
- **Lexical orthographic matching task**: During this task, the children were given every five seconds two two-syllable words, which were either identical or different. Once the two words were read, the child decided whether they are equal by pressing the right hand button, or spelled differently by pressing the one in the left hand. The words and pseudowords used in the two tasks listed so far were selected in accordance with the standardized reading test PROLEC-R.
- **Semantic categorisation task**: Three words were displayed every five seconds. Two of them were from the same semantic category and were displayed on the top of the screen. The third word, displayed in the bottom, either belonged to the same semantic category or did not. The child pushed the right hand button if he/she decided that the all the words shared the same semantic category, or the left hand button in the opposite case.

During the rest phases, strings of signs were displayed on the screen, so that no reading stimulus could occur. The Fig. 1 depicts the experimental design of this database acquisition.

Table 2
Scanning Parameters used for this study.

Parameters	Value
TR/TE	3000 / 30 ms
Matrix size	96 × 96
flip angle	90 degrees
field of view	230 × 230 cm
number of slices	25
slice thickness	4 mm with no gap
number of volumes	90
NSA	1
Total acquisition time	4'39"

The scanning protocol was conducted using Philips Achieva 3.0-T MRI system of 32-channel coil (Philips Medical Systems, Best, Netherlands). For the three reading tasks, BOLD functional images were acquired using an axial single shot EPI method block design (9 blocks: 5 Resting and 4 Reading) [17]. The chosen scanning parameters are presented in Table 2.

2.2. Proposed framework

First of all, the preprocessing step was given a high attention since the raw database contains many defects which reduce the efficiency of the intersubject and intrasubject variability. The preprocessing relies on a series of transformations in order to bring all the subject brains into one single model which will enable voxels comparison between each subject. This step was all conducted using SPM12 software with Matlab 2018b environment. Then, once the 3D volumes containing the activated areas were retrieved after the preprocessing step, they were fed to a 3D Convolutional Neural Network which was trained to distinguish between the differ-

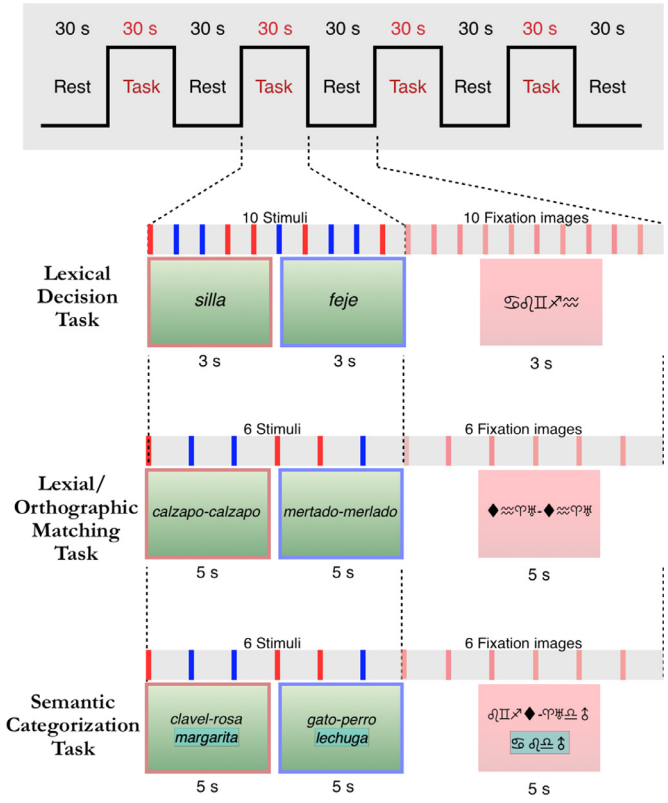

Fig. 1. The experimental design of the database acquisition [17]: During the reading blocks, a two-syllable word was displayed each 3 seconds in Lexical decision task, either real word (silla in this example, which means chair) or pseudoword (feje, which does not have a meaning). Or, in Orthographic marching task, two two-syllable words displayed every 5 seconds, either identical (calzapo - calzapo) or dissimilar (mertado-merlado). For the semantic categorization task, three words were displayed every 5 seconds, two words belong to the same semantic category and the third word either belongs also (e.g. clavel, rosa, margarita meaning carnation, rose and daisy in Spanish) or does not belong to the same semantic category (e.g. gato, perro, lechuga meaning cat, dog and lettuce in Spanish).

ent areas of activation depending on the class it belongs to: Non dyslexic (TDR and MVR) or Dyslexic (DXR). Based on the study conducted by Saralegui. et al [17], the pattern of activation while reading in Monocular vision group seemed similar to that in control children with no vision disorders, and different from that in dyslexic children. This is because dyslexia is, at its core, a problem with phonological processing which is related to a neurological disorder, not to vision impairments. For this reason, we merged the two groups (TDR and MVR) into one class of Non dyslexic, and kept dyslexic children in the second class. Fig. 2 sketches our processing workflow for dyslexia detection. Fig. 2 sketches our processing workflow for dyslexia detection.

2.2.1. DICOM to NIFTI conversion

Fistly, all the DICOM files were organized into 3 folders of each subject using the metadata in each DICOM image (Lexical decision (2250 scans), Orthographic matching (2250 scans) and Semantic categorization (2250 scans)). Then, the DICOM images in each folder were converted into NIFTI volumes which is the standard format that is processable by SPM software. This software package was created for the analysis of brain image data. It was used to conduct all the preprocessing steps. This conversion generated 90 volumes in each folder. In fact, 2250 scans are a concatenation of 25 brain layers acquired during a period of 270 s and scanned each 3 s (2250=25*270/3). Since the test was composed of 9 periods (5 resting and 4 reading), then each one of these periods contains 10 volumes, as shown in Fig. 2.

2.2.2. Adjustment of head motion

Head motion during fMRI scan acquisition can lead to errors in further analysis of brain voxels between subjects. The headers were altered for each of the input images to reflect the relative orientations of the head during the scanning. For each subject, the 90 volumes of all the 3 tests (sessions) were realigned to each other. Firstly, the first scans from each session were aligned. Later, the images in each session were aligned to the first image of the session.

2.2.3. Normalization

The brains come in different shapes and forms. These differences are likely to lead to an inherently biased findings. When all the scans were aligned, an image of the same sequence of image was used to estimate some warping parameters which will map it onto a template ATLAS. Then the rest of the images were warped accordingly.

2.2.4. Smoothing

The aim of this step is to suppress noise and reduce effects caused by the previous transformations. The chosen full width at half maximum (FWHM) of the Gaussian smoothing kernel was 4mm.

2.2.5. GLM design matrix and parameters

Now that the full database has been spatially preprocessed, the following steps consisted in conducting the statistical analysis of the brain volumes in order to detect the activated regions during the reading tasks for each subject in each one of the three reading tasks. For each subject and test, the GLM design matrix was defined by introducing the parameters of the experimental design. This part was performed using "1st level analysis" batch of the SPM software. Once the GLM matrix defined, the GLM parameters were estimated using Variational Bayes (VB) [37] using the "estimate" batch.

2.2.6. Generation of statistical parametric maps

The contrasts were specified using "results" button of the software interface in order to generate Statistical Parametric Maps (SPMs). Since our approach is to use the brain areas of activation to classify the subjects, the analysis conducted by Saralegui. et al [17] was used as a primary reference for the selection of the specific brain areas to include in the study. In fact, the selection of only the brain parts where a difference between subjects was noticed will remove any information likely to reduce the model's learning efficiency.

For Lexical decision task, as shown in fig 3, the chosen areas were:

- Left/right Broca's areas (BA 45 and BA 44)
- Left/right MTG (BA 21)
- Left/right VWFA 1/2 (BA 37)
- Left/right VWFA 3 (BA 20)
- Left Wernicke's area (BA 22)

For Orthographic matching task, as shown in Fig. 4, the chosen areas were:

- Right Broca's areas (BA 45 and BA 44)
- Left Broca's areas (BA 44)
- Left/right MTG (BA 21)
- Left/right precuneus (BA 19)
- Left V5-MT (BA 39)

For Semantic categorization task, as shown in Fig. 5, the chosen areas were:

- Left/right Broca's areas (BA 45 and BA 44)

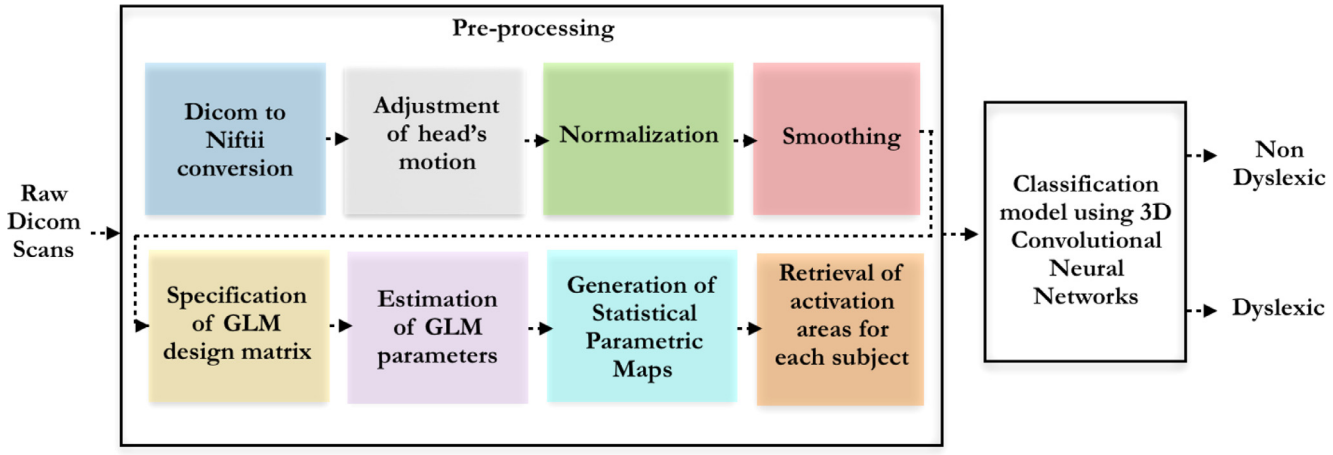

Fig. 2. Proposed architecture for dyslexia detection with fMRI scans using deep learning techniques.

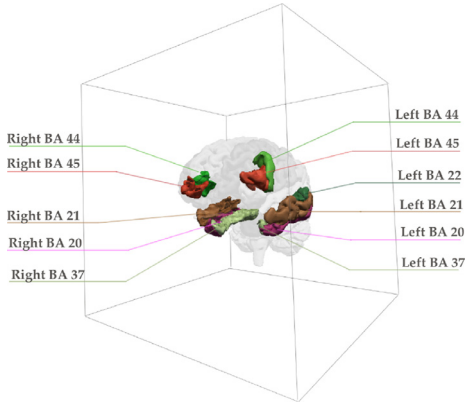

Fig. 3. Surface rendering of the locations of the selected brain regions for lexical decision task.

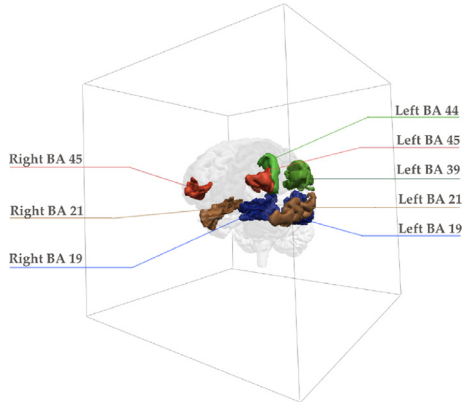

Fig. 4. Surface rendering of the locations of the selected brain regions for orthographic matching task.

- Left/right MTG (BA 21)
- Left V5-MT (BA 39)
- Left/right Wernicke's area (BA 22)
- Left/right precuneus (BA 19)

2.2.7. Retrieval of activation areas

Once the brain areas listed above were selected to mask the brain activation areas, the NIFTII files containing the slices of the brain, each with the activated areas were saved using the in-

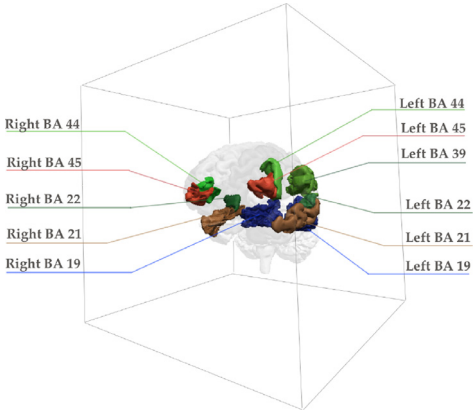

Fig. 5. Surface rendering of the locations of the selected brain regions for semantic categorization task.

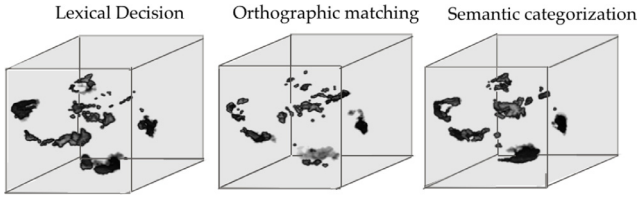

Fig. 6. Examples of the output of preprocessing step for the three reading tasks of a non-dyslexic child.

teractive window of the software. The size of these volumes is 79x95x95x3, as shown in Fig. 6.

As an output of the preprocessing phase, a total of 165 volumes were created: 57 volumes (19*3) for dyslexic class and 108 volumes (36*3) for non-dyslexic class.

2.2.8. 3D convolutional neural networks

The massive interest in artificial intelligence for learning data representations has enabled a new way of handling statistical modelling in neuroimaging, by virtue of computing infrastructures improvement. Of particular interest to us is the potential of 3D convolutional neural networks (CNN) to make a distinction between brain activation of children with dyslexia and those without, and thence enabling an early detection of this disorder simply from the analysis of fMRI scans during reading stimulus. As 2D convolutional neural networks have shown great success on 2D images,

Table 3
Summary of the proposed architecture with detailed parameters and input and output shapes.

Input	Layer (type)	Remarks	Output shape	Parameters #
Input 1 (95,79,79,3)	Conv3D_11	Feature maps = 8 kernel_size=(5,5,5) activation='relu' pool_size=(2, 2, 2)	(95,79,79)	3008
	Max_pooling3D_11	strides=(2,2,2)	(47,39,39)	0
	Conv3D_12	Feature maps = 16 kernel_size=(3,3,3) activation='relu' pool_size=(2, 2, 2)	(47,39,39)	3472
	Max_pooling3D_12	strides=(2,2,2)	(23,19,19)	0
	Flatten_1	flatten	132,848	0
	Dense_11	Units=32	32	4,251,168
	Dropout1	p=0.5	32	0
	Dense_12	Units=8	8	264
Input 2 (95,79,79,3)	Conv3D_21	Feature maps = 8 kernel_size=(5,5,5) activation='relu' pool_size=(2,2,2)	(95,79,79)	3008 0
	Max_pooling3D_21	strides = (2,2,2)	(47,39,39)	0
	Conv3D_22	Feature maps = 16 kernel_size=(3,3,3) activation='relu' pool_size=(2, 2, 2)	(47,39,39)	3472
	Max_pooling3D_22	strides = (2,2,2)	(23,19,19)	0
	Flatten_2	flatten	132,848	0
	Dense_21	Units=32	32	4,251,168
	Dropout2	p=0.5	32	0
	Dense_22	Units=8	8	264
Input 3 (95,79,79,3)	Conv3D_31	Feature maps = 8 kernel_size=(5,5,5) activation='relu' pool_size=(2, 2, 2))	(95,79,79)	3008
	Max_pooling3D_31	strides = (2,2,2)	(47,39,39)	0
	Conv3D_32	Feature maps = 16 kernel_size=(3,3,3) activation='relu' pool_size=(2, 2, 2)	(47,39,39)	3472
	Max_pooling3D_32	strides = (2,2,2)	(23,19,19)	0
	Flatten_3	flatten	132,848	0
	Dense_31	Units=32	32	4,251,168
	Dropout3	p=0.3	32	0
	Dense_32	Units=8	8	264
	Concat	Concatenate (Dense_12, Dense_22,Dense_32)	24	0
	Dense	activation='sigmoid'	1	25

applying a 3D CNN on the 3D image of the whole brain will capture local 3D patterns which may boost our classification results. The 3D CNNs function in the same way as 2D CNNs, with the exception of convolution kernels that are expanded to three dimensions. The architecture of 3D CNN is composed of stacked layers of 3D convolutions and 3D maxpooling layers, followed by flatten layer, dense layers and output prediction layer.

- 3D convolution layer: It represents the core layer of a CNN architecture. A filter with learnable weights slides over the input while moving in 3-direction (height, width, depth of the image) to calculate the feature representations, and produces a weighted sum as the output. The weighted sum is the feature space that represents the input for the next layers. The Fig. 7 shows the concept of the sliding 3D window of size (3x3x3) over a (9x9x9) matrix with stride=(1,1,1) and no zero padding. The output size is (7x7x7).
- 3D maxpooling layer: This layers extends the functionality of a max pooling layer to a third dimension. It down-samples the input data by dividing it into cuboidal regions and computing the maximum of each region. The purpose of its usage is to gradually decrease the spatial size of the representation and the amount of parameters learned in the network, and hence controlling overfitting.

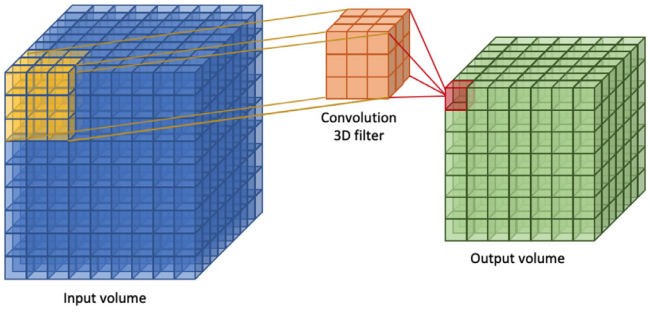

Fig. 7. Illustration of 3D convolution applied on a (9x9x9) input volume with a (3x3x3) filter sliding through the 3D space, and resulting in a (7x7x7) output volume.

The proposed framework, as shown in Fig. 8 and detailed in Table 3, for each one of the three input volumes, is composed of two 3D convolution layers, each one followed by a 3D max pooling layer. Then, a flatten layer followed by a dense layer with

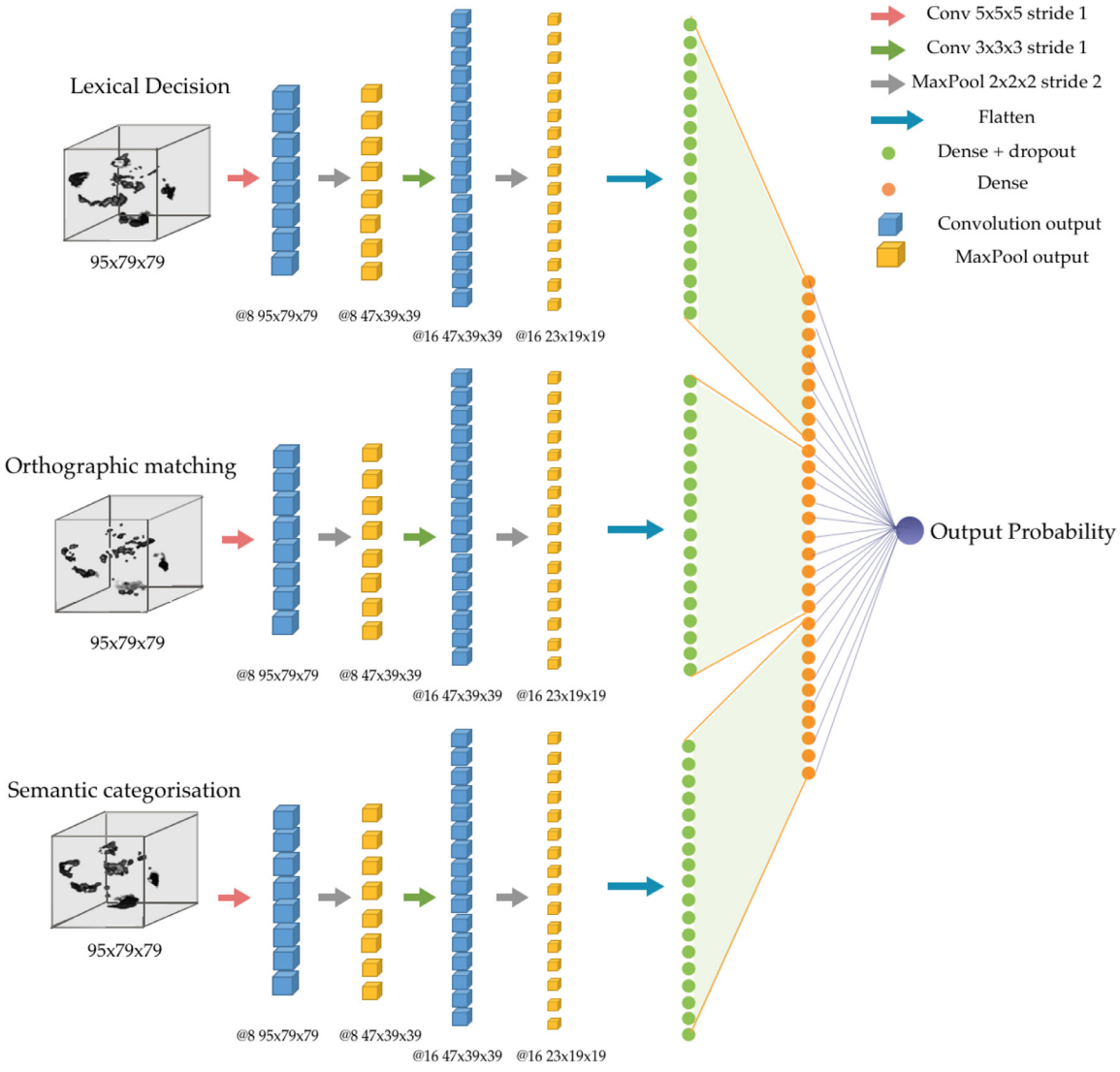

Fig. 8. Proposed 3D Convolutional Neural Network architecture for the classification of brain activation of dyslexic children.

dropout layer of 0.3. After the three dense layers are concatenated in a second dense layer, the output classification is given in the output layer using sigmoid function. Our architecture was implemented using Keras 2.1 and TensorFlow 1.12 libraries with dual Nvidia Geforce GTX 1080 Ti graphical processing unit (GPU) support. Initially, we set initial hyperparameters as presented by Zou, Liang, et al. [42] due to a fair similarity between our proposed architectures. Then, after tuning the hyperparameters in a 4-fold cross validation protocol, we trained our model using the Adam optimizer and a learning rate of 1e−5, a batch size of 8, and 15 epochs were chosen using early stopping callback. The database is composed of 165 3D volumes (55 children * 3 reading tasks). The balanced splitting was done by keeping 33 3D volumes (33 volumes = 11 children * 3 reading tasks) for testing, which represents 25% of the database, and kept the other 75% (132 volumes = 44 children * 3 reading tasks) for training and validation. Due to the size of data used in this study, which was relatively small for a deep learning strategy, we used 4-fold cross validation to avoid overfitting. Thus, during each fold, the model was trained on 99 3D volumes (33 children * 3 reading tasks), and validated on 33 3D volumes (11 children * 3 reading tasks).

3. Results and discussion

3.1. Validation metrics

Our model classification was evaluated on the testing set using five performance measures: overall accuracy, sensitivity (recall), specificity, precision and F1-score, using python scikit-learn module [26]. Four metrics were used to measure the performance of our approach: The True Positive (TP) refers to those volumes that were correctly classified as dyslexic and the False Positive (FP) represents the non-dyslexic volumes mistakenly classified as dyslexic. Whereas, the False Negative (FN) represents the activation volumes belonging to dyslexic class that were classified as non-dyslexic, and the True Negative (TN) refers to the non-dyslexic activation volumes correctly classified as non-dyslexic. From these values, we calculate the following performance measures:

- Overall accuracy: It is the ratio of the number of activation volumes accurately classified out of the total number of testing volumes.

$$Overall\ Accuracy = \frac{\mathbf{TP} + \mathbf{FN}}{\mathbf{TP} + \mathbf{TN} + \mathbf{FP} + \mathbf{FN}} \quad (1)$$

Table 4
Results of the dyslexia detection on a set of 11 participants(4 dyslexic and 7 non-dyslexic).

		Predicted class	
		Dyslexic	Non dyslexic
Actual class	Dyslexic	3	1
	Non dyslexic	2	5
Evaluation metric		Value	
Sensitivity		75%	
Specificity		71.43%	
Precision		60%	
F1-score		67%	
Overall accuracy		72.73%	

- Sensitivity: Also named "recall", It represents the ratio of brain activation volumes accurately classified as dyslexic out of the total number of dyslexic children.

$$Sensitivity = \frac{\mathbf{TP}}{\mathbf{TP} + \mathbf{FN}} \tag{2}$$

- Specificity: It represents the ratio of non-dyslexic children that are correctly identified out of the total number of non-dyslexic children.

$$Specificity = \frac{\mathbf{TN}}{\mathbf{TN} + \mathbf{FP}} \tag{3}$$

- Precision: It represents the ratio of dyslexic brain activation accurately classified out of the union of predicted same-class volumes.

$$Precision = \frac{\mathbf{TP}}{\mathbf{TP} + \mathbf{FP}} \tag{4}$$

- F1-score: this is the harmonic mean between precision and recall

$$F1 - score = \frac{\mathbf{2} * \mathbf{Precision} * \mathbf{Recall}}{\mathbf{Precision} + \mathbf{Recall}} \tag{5}$$

3.2. Results and discussion

The selected hyperparameters were chosen based on the best mean accuracy, which was 75% with the previously stated hyperparameters. Then, the model was trained on all the 132 volumes (44 children) and tested on the testing set. The model was able to reach an overall accuracy of 72,73%, a specificity of 71.43%, a precision of 60% and an F1-score of 67% in dyslexia detection as shown in Table 4.

According to the state of the art results, convolutional neural networks have proven to be efficient in extracting important features and accurately clustering them in the 2-dimensional domain [18,19,23]. Nonetheless, there have been very few contributions in which 3D-CNN has been deployed to classify and predict disorders using volumetric neuroimaging data [38–41], our developed approach for dyslexia detection through brain activation analysis has shown that 3D CNN can also learn spatial features in 3D volumes containing brain activation areas. Tamboer, P., et al. [54], an SVM classifier was trained on 41 preprocessed brain scans to classify them based on their anatomical differences. They achieved, on 60 dyslexic individuals (7%) and 816 non dyslexic (93%), a total sensitivity of 67% and a specificity of 59%. Our method applied on a limited amount of data has proven to be able to extract the underlying features from the 3D volumes of brain activation and fairly classifying them. It is to be noted that because of the limited number of volumes for testing, the values of metrics highly fluctuate with only one more brain correctly or incorrectly classified.

However, our study has some limitations. First of all, the number of participants in the study is limited. Hence, acquiring larger samples using different experiments is needed to reach higher levels of evidence. Moreover, using SPM software, we were able to select the brain regions corresponding to reading and language comprehension. Nonetheless, we believe that there are subregions in these areas which can better discriminate the differences in activation, and hence reducing confusion for the learning. Also, in this study, we did not include the differentiation between different subtypes of dyslexia, where it was found that only the subtype of dyslexia with poor phonological awareness and magnocellular skills demonstrated an increased gray matter volume in the right putamen and the left cerebellum compared to controls, while the other two subtypes of dyslexia did not show differences at these regions [36]. Hence, the lack of this differentiation may also be hindering an efficient learning.

4. Conclusion

The purpose of this paper is to detect dyslexic children by means of deep learning neural network from the 3D volumes of brain activation. Unlike the state of the art methods that mostly work on the whole brain fMRI scans (either 2D or 3D), we propose a method which only targets the brain activation areas in order to tackle our classification problem. To prepare the input data, the fMRI scans were passed through a serie of preprocessing steps using SPM12 software, which are: Dicom to Niftii conversion, adjustment of head motion to reduce intersubject vaiability, normalization to a template Atlas in order to reduce intrasubject variability and the application of a smoothing filter to suppress noise. Then, statistical parametric maps were generated using the same software in order to retrieve the activated brain areas. For the purpose of reducing brain activation areas which may be present in all the participants and hence will reduce the efficiency of feature learning, we decided to keep only the brain areas responsible for reading and language comprehension, as presented by Saralegui et al [17]. As the participants have gone through three different reading paradigms, each participant had three brain activation volumes which were fed to the designed neural network. The presented architecture composed of three parallel 3D CNN combined with a dense layer has enabled the classification of dyslexic children with an overall accuracy of 72,73% and specificity of 75%. Due to the limited number of participants, we used 4-fold cross validation method to assess the generalizability of our model and control overfitting. Hence, future work will be focused on acquiring more data and conducting a deeper analysis of subregions from the selected brain areas where the difference in activation is even more significant. Furthermore, the combination of the collected data during the reading paradigms (reading accuracy, reading speed, etc) with the current model will be added in order to improve the performance of the system. When better results will be achieved, the features learned will be used for the classification of other neurological conditions such as migraine using transfer learning.

Declaration of Competing Interest

None.

Acknowledgments

This project has been partially funded by the Basque government, and eVida certified Group IT905-16 for publication fees and grants for research projects of the Health Department (2019222044 and 2018222002). The authors would like to thank Osatek (Magnetic Resonance Unit, Galdakao, Spain) for the data provided in order to carry out this work. Acknowledgment to Basque country government that partially funded this project with IT905-16, 2019222044 and 2018222002 grants.

References

[1] S.M. Handler, W.M. Fierson, Section on ophthalmology, council on children with disabilities, american academy of ophthalmology, american association for pediatric ophthalmology and strabismus, American Association of Certified Orthoptists (2011) 2010–3670. Learning disabil- ities, dyslexia, and vision. Pediatrics 127, e818-e856. doi: 10.1542/peds.

[2] D.J. Hodgetts, J.W. Simon, T.A. Sibila, D.M. Scanlon, F.R. Vellutino, Normal reading despite limited eye movements, J. AAPOS 2 (1998) 182–183, doi:10.1016/S1091-8531(98)90011-8.

[3] A.M. Galaburda, G.F. Sherman, G.D. Rosen, F. Aboitiz, N. Geschwind, Developmental dyslexia: four consecutive patients with cortical anomalies, Ann. Neurol. 18 (1985) 222–233, doi:10.1002/ana.410180210.

[4] S.E. Shaywitz, B.A. Shaywitz, K.R. Pugh, R.K. Fulbright, R.T. Constable, W.E. Mencl, Functional disruption in the organization of the brain for reading in dyslexia, Proc. Natl. Acad. Sci. USA 95 (1998) 2636–2641, doi:10.1073/pnas.95.5.2636.

[5] M.J. Snowling, C. Hulme, Evidence-based interventions for reading and language difficulties: Creating a virtuous circle, Br. J. Educ. Psychol. 81 (2011) 1–23, doi:10.1111/j.2044-8279.2010.02014.x. Pt 1

[6] E. Paulesu, J.F. Démonet, F. Fazio, E. McCrory, V. Chanoine, N. Brunswick, Dyslexia: cultural diversity and biological unity, Science 291 (2001) 2165–2167, doi:10.1126/science.1057179.

[7] P. Tallal, S.L. Miller, G. Bedi, G. Byma, X. Wang, S.S. Nagarajan, Language comprehension in language-learning impaired children improved with acoustically modified speech, Science 271 (1996) 81–84, doi:10.1126/sci- ence.271.5245.81.

[8] R.I. Nicolson, A.J. Fawcett, P. Dean, Dyslexia development and the cerebellum, Trends Neurosci. 24 (2001) 508–511, doi:10.1016/S0166-2236(00) 01896-8.

[9] N.W. Roach, J.H. Hogben, Attentional modulation of visual processing in adult dyslexia a spatial-cuing deficit, Psychol. Sci. 15 (2004) 650–654, doi:10.1111/j.0956-7976.2004.00735.x.

[10] A. Facoetti, M. Zorzi, L. Cestnick, M. Lorusso, M. Molteni, P. Paganoni, The relationship between visuo-spatial attention and non word reading in developmental dyslexia, Cognit. Neuropsychol. 23 (2006) 841–855, doi:10.1080/02643290500483090.

[11] M. Bosse, M. Tainturier, S. Valdois, Developmental dyslexia: the visual attentions pan deficit hypothesis, Cognition 104 (2007) 198–230, doi:10.1016/j.cognition.2006.05.009.

[12] M. Lobier, R. Zoubrinetzky, S. Valdois, The visual attention span deficit in dyslexia is visual and not verbal, Cortex 48 (2012) 768–773, doi:10.1016/j.cortex.2011.09.003.

[13] Z. Wang, X. Yan, Y. Liu, G.J. Spray, Y. Deng, F. Cao, Structural and functional abnormality of the putamen in children with developmental dyslexia, Neuropsychologia 130 (2019) 26–37.

[14] M.S. Livingstone, G.D. Rosen, F.W. Drislane, A.M. Galaburda, Physiological and anatomical evidence fora magnocellular defect in developmental dyslexia, Proc. Natl. Acad. Sci. USA 88 (1991) 7943–7947, doi:10.1073/pnas.88.18.7943.

[15] J.F. Stein, V. Walsh, To see but not to read; the magnocellular theory of dyslexia, Trends Neurosci. 20 (1997) 147–152, doi:10.1016/S0166-2236(96)01005-3.

[16] T.R. Vidyasagar, K. Pammer, Dyslexia: a deficit in visuo-spatial attention,not in phonological processing, Trends Cognit. Sci. 14 (2009) 57–63, doi:10.1016/j.tics.2009.12.003.

[17] I. Saralegui, J.M. Ontañón, B. Fernandez-Ruanova, B. Garcia-Zapirain, A. Basterra, E.J. Sanz-Arigita, Reading networks in children with dyslexia compared to children with ocular motility disturbances revealed by fMRI, Front. Hum. Neurosci. 8 (2014) 936.

[18] A. Payan, G. Montana, Predicting alzheimer's disease: a neuroimaging study with 3d convolutional neural networks, 2015, arXiv preprint: 1502.02506

[19] E. Hosseini-Asl, G. Gimel'farb, A. El-Baz, Alzheimer's dis- ease diagnostics by a deeply supervised adaptable 3d convolutional network, 2016, arXiv preprint: 1607.00556

[20] H. Choi, K.H. Jin, Fast and robust segmentation of the striatum using deep convolutional neural networks, Journal of Neuro- science Methods 274 (2016) 146–153. Dou, Q., Chen, H., Yu, L., Zhao, L., Qin, J., Wang, D., Mok, V. C., Shi, L., Heng, P.-A., 2016c. [23] Automatic detection of cerebral micro-bleeds from MR images via 3D convolutional neural networks. IEEE Trans Med Imaging 35, 1182-1195.

[21] M. Ghafoorian, N. Karssemeijer, T. Heskes, M. Bergkamp, J. Wissink, J. Obels, K. Keizer, F.E. de Leeuw, B. van Ginneken, E. Marchiori, B. Platel, Deep multi-scale location- aware 3d convolutional neural networks for automated detection of lacunes of presumed vascular origin, NeuroImage: Clinical (2017). In press

[22] D. Nie, H. Zhang, E. Adeli, L. Liu, D. Shen, 3d deep learning for multi-modal imaging-guided survival time prediction of brain tumor patients, in: Med Image Comput Comput Assist Interv. Vol. 9901 of Lect Notes Comput Sci., 2016, pp. 212–220.

[23] R. Li, W. Zhang, H.-I. Suk, L. Wang, J. Li, D. Shen, S. Ji, Deep learning based imaging data completion for improved brain disease diagnosis, in: Med Image Comput Comput Assist Interv. Vol. 8675 of Lect Notes Comput Sci., 2014, pp. 305–312.

[24] K. Bahrami, F. Shi, I. Rekik, D. Shen, Convolutional neural network for reconstruction of 7t-like images from 3t MRI using appearance and anatomical features, in: DLMIA. Vol. 10008 of Lect Notes Comput Sci., 2016, pp. 39–47.

[25] M. Simonovsky, B. Gutierrez-Becker, D. Mateus, N. Navab, N. Komodakis, A deep metric for multimodal registration, in: Med Image Comput Comput Assist Interv. Vol. 9902 of Lect Notes Comput Sci., 2016, pp. 10–18.

[26] S. Ashish, R. Jain, Scikit-learn: machine learning in python, J. Mach. Learn. Res. 12 (10) (2012) 2825–2830.

[27] H. Chougrad, H. Zouaki, O. Alheyane, Deep convolutional neural networks for breast cancer screening, Comput. Methods Programs Biomed. 157 (2018) 19–30.

[28] M.A. Al-masni, M.A. Al-antari, J.M. Park, G. Gi, T.Y. Kim, P. Rivera, T.S. Kim, Simultaneous detection and classification of breast masses in digital mammograms via a deep learning YOLO-based CAD system, Computer methods and programs in biomedicine 157 (2018) 85–94.

[29] Z. Zhu, E. Albadawy, A. Saha, J. Zhang, M.R. Harowicz, M.A. Mazurowski, Deep learning for identifying radiogenomic associations in breast cancer, Comput. Biol. Med. 109 (2019) 85–90.

[30] M.F. Bobo, S. Bao, Y. Huo, Y. Yao, J. Virostko, A.J. Plassard, B.A. Landman, Fully convolutional neural networks improve abdominal organ segmentation, Medical Imaging 2018: Image Processing (Vol. 10574, p. 105742V). International Society for Optics and Photonics, 2018.

[31] H. Hu, N. Pan, J. Wang, T. Yin, R. Ye, Automatic segmentation of left ventricle from cardiac MRI via deep learning and region constrained dynamic programming, Neurocomputing 347 (2019) 139–148.

[32] M.R. Avendi, A. Kheradvar, H. Jafarkhani, A combined deep-learning and deformable-model approach to fully automatic segmentation of the left ventricle in cardiac MRI, Med. Image Anal. 30 (2016) 108–119.

[33] M.A. Al-Masni, M.A. Al-antari, M.T. Choi, S.M. Han, T.S. Kim, Skin lesion segmentation in dermoscopy images via deep full resolution convolutional networks, Comput. Methods Programs Biomed. 162 (2018) 221–231.

[34] S. Zahia, D. Sierra-Sosa, B. Garcia-Zapirain, A. Elmaghraby, Tissue classification and segmentation of pressure injuries using convolutional neural networks, Comput. Methods Programs Biomed. 159 (2018) 51–58.

[35] P.M. Burlina, N.J. Joshi, E. Ng, S.D. Billings, A.W. Rebman, J.N. Aucott, Automated detection of erythema migrans and other confounding skin lesions via deep learning, Comput. Biol. Med. 105 (2019) 151–156.

[36] K. Jednoróg, N. Gawron, A. Marchewka, S. Heim, A. Grabowska, Cognitive subtypes of dyslexia are characterized by distinct patterns of grey matter volume, Brain Struct. Funct. 219 (5) (2014) 1697–1707.

[37] W. Penny, S. Kiebel, K. Friston, Variational Bayesian inference for fMRI time series, NeuroImage 19 (3) (2003) 727–741.

[38] M.N.I. Qureshi, S. Ryu, J. Song, K.H. Lee, B. Lee, Evaluation of functional decline in Alzheimer's dementia using 3d deep learning and group ICA for rs-fMRI measurements, Front. Aging Neurosci. 11 (2019).

[39] M. Khosla, K. Jamison, A. Kuceyeski, M.R. Sabuncu, Ensemble learning with 3d convolutional neural networks for functional connectome-based prediction, NeuroImage (2019).

[40] K.R. Kruthika, H.D. Maheshappa, Alzheimer's disease neuroimaging initiative, in: CBIR system using Capsule Networks and 3D CNN for Alzheimer's disease diagnosis. Informatics in Medicine Unlocked, 14, 2019, pp. 59–68.

[41] X.W. Gao, R. Hui, Z. Tian, Classification of CT brain images based on deep learning networks, Comput. Methods Programs Biomed. 138 (2017) 49–56.

[42] L. Zou, J. Zheng, C. Miao, M.J. Mckeown, Z.J. Wang, 3d CNN based automatic diagnosis of attention deficit hyperactivity disorder using functional and structural MRI, IEEE Access 5 (2017) 23626–23636.

[43] G. Cheng, P. Zhou, J. Han, Learning rotation-invariant convolutional neural networks for object detection in VHR optical remote sensing images, IEEE Trans. Geosci. Remote Sens. 54 (12) (2016) 7405–7415.

[44] D. Sarikaya, J.J. Corso, K.A. Guru, Detection and localization of robotic tools in robot-assisted surgery videos using deep neural networks for region proposal and detection, IEEE Trans. Med. Imaging 36 (7) (2017) 1542–1549.

[45] J. Han, D. Zhang, G. Cheng, L. Guo, J. Ren, Object detection in optical remote sensing images based on weakly supervised learning and high-level feature learning, IEEE Trans. Geosci. Remote Sens. 53 (6) (2014) 3325–3337.

[46] M.A. Al-Masni, M.A. Al-antari, M.T. Choi, S.M. Han, T.S. Kim, Skin lesion segmentation in dermoscopy images via deep full resolution convolutional networks, Comput. Methods Programs Biomed. 162 (2018) 221–231.

[47] X. Zhao, Y. Wu, G. Song, Z. Li, Y. Zhang, Y. Fan, A deep learning model integrating FCNNs and CRFs for brain tumor segmentation, Med. Image Anal. 43 (2018) 98–111.

[48] K. Kamnitsas, C. Ledig, V.F. Newcombe, J.P. Simpson, A.D. Kane, D.K. Menon, B. Glocker, Efficient multi-scale 3d CNN with fully connected CRF for accurate brain lesion segmentation, Med. Image Anal. 36 (2017) 61–78.

[49] J. Dolz, C. Desrosiers, I.B. Ayed, 3d fully convolutional networks for subcortical segmentation in MRI: a large-scale study, NeuroImage 170 (2018) 456–470.

[50] Y. Gu, X. Lu, L. Yang, B. Zhang, D. Yu, Y. Zhao, T. Zhou, Automatic lung nodule detection using a 3d deep convolutional neural network combined with a multi-scale prediction strategy in chest CTs, Comput. Biol. Med. 103 (2018) 220–231.

[51] H. Jiang, F. Gao, X. Xu, F. Huang, S. Zhu, Attentive and ensemble 3d dual path networks for pulmonary nodules classification, Neurocomputing (2019).

[52] M.N.I. Qureshi, J. Oh, B. Lee, 3d-CNN based discrimination of schizophrenia using resting-state fMRI, Artif. Intell. Med. (2019).

[53] K. Oh, W. Kim, G. Shen, Y. Piao, N.I. Kang, I.S. Oh, Y.C. Chung, Classification of schizophrenia and normal controls using 3d convolutional neural network and outcome visualization, Schizophrenia Res. 212 (2019) 186–195.

[54] P. Tamboer, H.C.M. Vorst, S. Ghebreab, H.S. Scholte, Machine learning and dyslexia: Classification of individual structural neuro-imaging scans of students with and without dyslexia, NeuroImage 11 (2016) 508–514.